



Simulation of Solar Cell Device Performance Based on Hydrogenated Microcrystal Silicon ($\mu\text{c-Si:H}$) With *Finite Element Method* (FEM)

La Ode Asmin^{1,*}), La Isa²

^{1,2}Physics Education Kendari State Islamic Institute, Jln Sultan Qaimuddin No 17, Kendari Southeast Sulawesi

*Corresponding email: fisikakuanta@gmail.com

Article info: Abstract

Sent:
17 April 2022
Revision:
25 July 2022
Accepted:
25 July 2022

Keywords:

Continuity,
FEMLAB,
MATLAB,
Poisson's
equation.
Solar cell device,

The structure and thickness of the solar cell device layer have a big impact on how well the solar cell works. There for, the aim of this study was to examine how hydrogenated microcrystalline silicon solar cells' thickness and device structure affected how well they work. Simulation or modeling of the structure in one dimension (1D) is used for the analysis. MATLAB programing was use to analyzed the simulation result. The optical band gap changes due to the influence of the structure, therefore the thickness of the p -, i and n layers are kept constant at 250 Å, 9000 Å and 250 Å respectively. The results showed that the maximum performance is obtained at the optical band gap, $E_{ci} = 1,39$ eV and the resulting power is 0.063465 Watt. Whereas in the simulation of the effect of the thickness on the i -layer, the optical band gap is set to a constant value of $E_{ci} = 1,4$ eV, while the thickness of the p -layer and n -layer is set to 250 Å. The results also indicate that the maximum performance is at the i -layer thickness of 9000 Å and the power generated is 0.063364 Watt.

© 2022 Mataram State Islamic University

INTRODUCTION

The oil-related energy crisis and rising air pollution is a big problem in this era. This calls for the urgent development of renewable energy sources that are limitless and save for the environment as alternative energy source. The aviability of alternative energy sources can reduce the production of greenhouse gases and consequently reduce global warming. Future sources of alternative energy for the world's energy supply are being invistigated, including the renewable energy technology [1]. The primary renewable energy source that may satisfy the growing global energy demand is solar energy. It is a plentiful, pure, lasting, and dependable source of energy. Solar cells are devices that use a photovoltaic process to transform solar radiation energy into electrical energy. Amorphous silicon-based solar cells are one of the most promising low-cost photovoltaic technologies. They are made of thin layers of the material. Because they may be produced on a variety of substrates, hydrogenated amorphous silicon (a-Si:H) and hydrogenated nanocrystalline silicon (nc-Si:H) thin films are frequently employed for multi-junction solar cell applications. These factors make a-Si:H and $\mu\text{c-Si:H}$ ideal for inexpensive technological equipment [2].

Hydrogenated amorphous silicon (a-Si:H) has a high absorpion coefficient in the solar visible spectrum. The a-Si:H band gap is about 1.75 eV only for absorpion in the infrared (IR) region. In the photoexcitation process, only photons with energies greater than the absorbing band gap can

contribute [5]. Therefore, a material with a lower band gap is required. One of the promising materials for this is hydrogenated microcrystalline silicon ($\mu\text{c-Si:H}$). It is supported that $\mu\text{c-Si:H}$ has a band gap lower than 1.1 eV, so it can be used as an absorber for absorption in the IR region [3].

Hydrogenated microcrystalline silicon material ($\mu\text{c-Si:H}$), which is a mixed-phase material between the crystalline phase and the amorphous phase. Some of the advantages of $\mu\text{c-Si:H}$ over a-Si:H include higher conductivity and lower hydrogen content. With these properties, the $\mu\text{c-Si:H}$ material is very suitable to be applied to solar cell devices with higher conversion efficiency and is more stable to high-intensity irradiation [4,5,6]. At high energy the absorption coefficient of $\mu\text{c-Si:H}$ is higher than that of a-Si:H. In order to obtain absorption and photogeneration coefficients in the appropriate wavelength range, the required layer thickness for $\mu\text{c-Si:H}$ must be kept within a few m. Based on the above considerations, the use of $\mu\text{c-Si:H}$ as a photogeneration layer in thin-layer solar cells will be needed in the next few years [4].

The process of converting light energy into electrical energy or vice versa in an optoelectronic device is physically quite complicated to study, because it involves many interrelated variables and influences each other's performance. To obtain an optoelectronic device structure that has optimum performance, an optimization process needs to be carried out, including through a theoretical study of the physical processes that occur when converting light energy into electricity or vice versa, followed by efficiency calculations. The advantage is that the process is cheap, while the disadvantage is that due to certain restrictions, the results obtained will deviate from the real thing [7].

The silicon-based thin films can be prepared as amorphous, microcrystalline or mixed phases, and it is known that the optical band gap can be precisely controlled. By controlling the optical gap, it is possible to fabricate high-efficiency multi-junction thin-film silicon solar cells that can become promising photovoltaic devices [8]. Therefore, in this study, optimization of the solar cell material parameters was carried out by simulating hydrogenated microcrystalline silicon ($\mu\text{c-Si:H}$) solar cell devices with variations in the optical band gap in the i -layer and the i -layer thickness.

RESEARCH METHODS

This type of research is a study of the physics of electronic materials. The method used in this research is literature study and simulation. The literature study method is used to study the physical phenomena that occur in the optoelectronic device under study, so that it can be represented in the simplest possible mathematical formulation and if possible obtain an exact equation solution and collect parameters from the device material. The simulation method is used to perform calculations to obtain a visual image showing the dependence of the performance of the optoelectronic device on the device structure, coating characteristics, and the parameters of the semiconductor material. The simulation process is carried out with the help of Femlab and Matlab software. The equations used in this study are as follows [9]:

Equation (1) is Poisson's :

$$\begin{aligned} \frac{\epsilon}{q} \nabla^2 \psi = & n_i (e^{\psi u} - e^{-\psi v}) - N_D + N_A \\ & - g_{Dmin} E_D \left[\exp\left(\frac{E_{mc} - E_c}{E_D}\right) \left\{ 1 - \left(\frac{2e^{-\psi v} + ce^{\psi u}}{e^{-\psi v} + e^{\psi uc}} \right) \left(\frac{n_i e^{-\psi v} + n_i ce^{\psi u}}{cN_c} \right)^{\frac{kT}{E_D}} \right\} \right. \\ & \left. + \exp\left(\frac{E_{mc} - E_c}{E_D}\right) \left\{ \left(\frac{e^{-\psi v}}{e^{-\psi v} + e^{\psi uc}} \right) \left(\frac{n_i e^{-\psi v} + n_i ce^{\psi u}}{N_v} \right)^{\frac{kT}{E_D}} \right\} \right] \\ & - g_{Amin} E_A \left[\exp\left(\frac{E_v - E_{mc}}{E_A}\right) \left\{ \left(\frac{ce^{-\psi v}}{ce^{-\psi v} + e^{\psi u}} \right) \left(\frac{cn_i e^{-\psi v} + n_i e^{\psi u}}{cN_v} \right)^{\frac{kT}{E_D}} - 1 \right\} \right. \\ & \left. + \exp\left(\frac{E_v - E_{mc}}{E_A}\right) \left\{ \left(\frac{e^{\psi u}}{cn_i e^{-\psi v} + e^{\psi u}} \right) \left(\frac{cn_i e^{-\psi v} + n_i e^{\psi u}}{N_c} \right)^{\frac{kT}{E_D}} \right\} \right] \end{aligned}$$

Equation (2) is electron distribution:

$$\begin{aligned}
 & -\nabla(\mu_n n \nabla \psi + D_n \nabla n) \\
 & = \frac{G_0 \alpha(\lambda)}{1 - P} (e^{-ax} + P e^{ax}) \\
 & - n_i (uv \\
 & - 1) cv \sigma_N \left[\frac{g_{Amin} E_A}{e^{\psi u} + e^{-\psi v} v c} \left\{ \left(\frac{n_i e^{\psi u} + c n_i e^{-\psi v}}{N_c} \right)^{\frac{kT}{E_A}} \exp\left(\frac{E_c - E_{mc}}{E_A}\right) \right. \right. \\
 & \left. \left. - \left(\frac{n_i e^{\psi u} + c n_i e^{-\psi v}}{c N_v} \right)^{\frac{kT}{E_A}} \exp\left(\frac{E_v - E_{mc}}{E_A}\right) \right\} \right. \\
 & \left. + \frac{g_{Dmin} E_D}{cn + p} \left\{ \left(\frac{n_i e^{\psi u} + c n_i e^{-\psi v}}{N_v} \right)^{\frac{kT}{E_A}} \exp\left(\frac{E_{mc} - E_v}{E_D}\right) \right. \right. \\
 & \left. \left. - \left(\frac{n_i e^{\psi u} + c n_i e^{-\psi v}}{c N_c} \right)^{\frac{kT}{E_A}} \exp\left(\frac{E_{mc} - E_c}{E_D}\right) \right\} \right]
 \end{aligned}$$

Equation (3) is hole distribution:

$$\begin{aligned}
 & -\nabla(\mu_p p \nabla \psi + D_p \nabla p) \\
 & = \frac{G_0 \alpha(\lambda)}{1 - P} (e^{-ax} + P e^{ax}) \\
 & - n_i (uv \\
 & - 1) cv \sigma_N \left[\frac{g_{Amin} E_A}{e^{\psi u} + e^{-\psi v} v c} \left\{ \left(\frac{n_i e^{\psi u} + c n_i e^{-\psi v}}{N_c} \right)^{\frac{kT}{E_A}} \exp\left(\frac{E_c - E_{mc}}{E_A}\right) \right. \right. \\
 & \left. \left. - \left(\frac{n_i e^{\psi u} + c n_i e^{-\psi v}}{c N_v} \right)^{\frac{kT}{E_A}} \exp\left(\frac{E_v - E_{mc}}{E_A}\right) \right\} \right. \\
 & \left. + \frac{g_{Dmin} E_D}{cn + p} \left\{ \left(\frac{n_i e^{\psi u} + c n_i e^{-\psi v}}{N_v} \right)^{\frac{kT}{E_A}} \exp\left(\frac{E_{mc} - E_v}{E_D}\right) \right. \right. \\
 & \left. \left. - \left(\frac{n_i e^{\psi u} + c n_i e^{-\psi v}}{c N_c} \right)^{\frac{kT}{E_A}} \exp\left(\frac{E_{mc} - E_c}{E_D}\right) \right\} \right]
 \end{aligned}$$

In this study, the optical band gap of the *i*-layer was varied between 1.39 eV to 1.43 eV, while the electron mobility and hole mobility remained at the values of 10 cm²/(V.s), and 5 cm²/(V.s, respectively).). The thickness of the *i*-layer is 9000 Å , while the *p*-layer and *n*-layer are both at a thickness of 250 Å . Simulations were carried out for variations in the thickness of the *i*-layer between 5000 Å to 9000 Å .

RESULTS AND DISCUSSION

Figure 1 The display of the Femlab software before and after the simulation process.

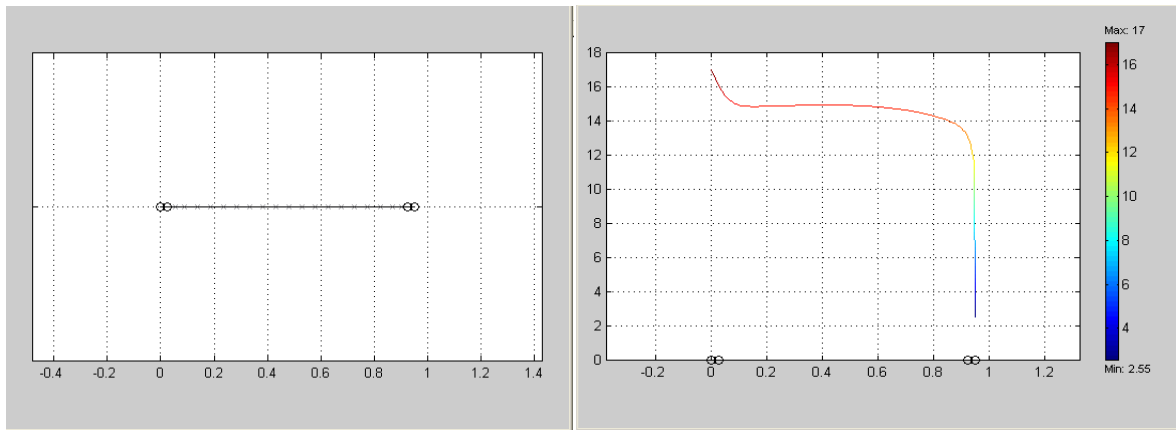


Figure 1. The display of the FEMLAB application before and after the simulation process (Printout from FEMLAB 2.0)

The characteristics of $\mu\text{-Si:H}$ solar cells with different energy gaps are 1.19 eV to 1.23 eV. It appears that the characteristics of solar cells are found at a smaller energy gap value (1.19 eV) [10]. The characteristics of a-Si:H solar cells have a very high dependence on the thickness of the i -layer, where the charge carrier generation mechanism starts in the layer [11]. Figure 2 shows the distribution profile of electrons and holes in $\mu\text{-Si:H}$ solar cells at different i -layer optical band gaps.

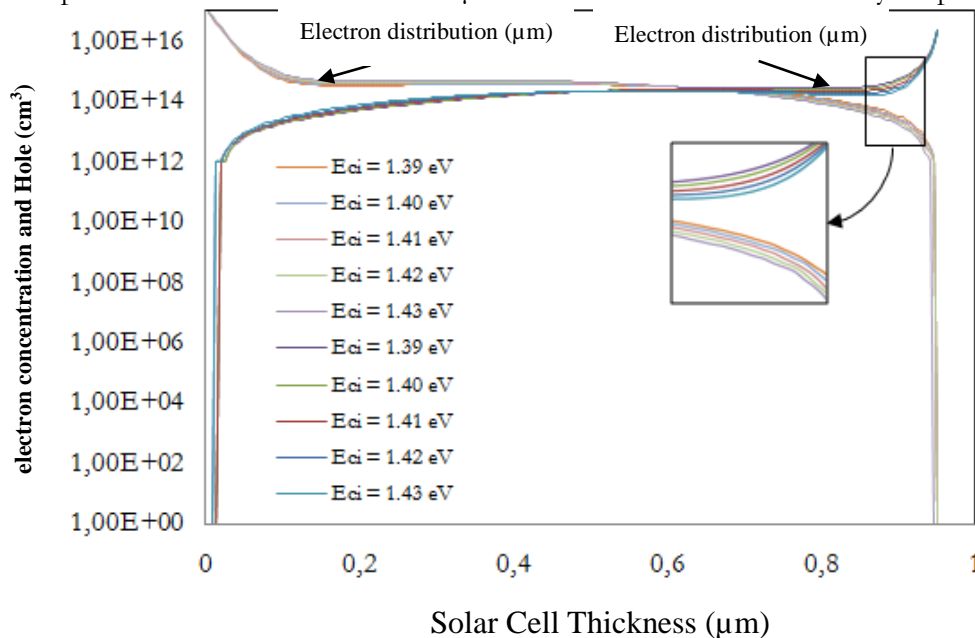


Figure 2 Electron and hole distribution profiles of $\mu\text{-Si:H}$ solar cell devices in the i -layer (E_{ci}) optical bandgap variation and the p -layer and n -layer optical band gaps remained at 1.42 eV and 1.5 eV

Based on Figure 2, it can be seen that the variation of the optical band gap which increases the concentration of holes starts from the p -layer, then the i -layer and finally to the n -layer. The electrons are well distributed in $\mu\text{-Si:H}$ solar cells with an i -layer which has a lower optical band gap width of 1.39 eV. This shows that the recombination process occurs more slowly at a higher optical band gap, especially in the n -layer region which has a high electron concentration. Meanwhile for the distribution of holes, which shows the relationship between hole concentration and the thickness of the solar cell, with variations in the value of the optical band gap which decreases the hole concentration starting from the p -layer, then the i -layer and finally to the n -layer. It appears that at a smaller optical band gap value of 1.39 eV, the hole concentration decreases faster. This shows that the concentration of holes, especially in the n layer, will quickly decrease if the recombination process occurs more quickly.

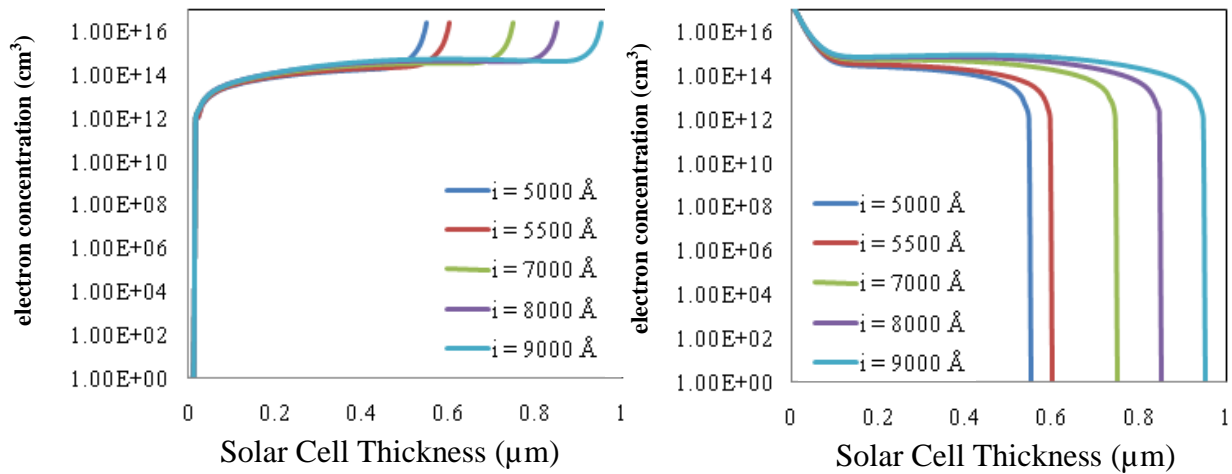


Figure 3. Electron distribution profile of $p-i-n$ μc -Si:H solar cell devices at (a) variation of i -layer thickness, with p -layer and n -layer thickness of 250 Å. And Hole concentration (b) i -layer thickness variation, with p -layer and n -layer thickness of 250 Å

Figure 3(a) depicts the i -layer thickness variation, which increases electron concentration from the p -layer to the i -layer and to the n -layer. From the figure, it can be understood that the highest electron concentration is in the n -layer. The variation in the thickness of the i -layer only affects the change in the value of the electron concentration in the i -layer where the thicker i -layer, $i = 9000$ Å has a higher electron concentration. While Figure 3(b) depicts the thickness variation in layer- i , which has decreased hole concentration from the p -layer to the i -layer and to the n -layer. From Figure 3 it can be seen that the highest hole concentration is in the p -layer. The variation of the thickness of the i -layer only affects the change in the value of the hole concentration in the i -layer where the thicker i -layer, $i = 9000$ Å has a higher hole concentration. This is caused by the effect of decreasing the rate of generation of charge carrier pairs in the thicker i -layer so that the recombination process decreases.

Figure 4(a) is an electrostatic potential profile for a solar cell device with an i -layer optical band gap variation with a fixed p -layer and n -layer optical band gap width at 1.42 eV and 1.5 eV with a $p-i-n$ layer thickness, respectively are 250 Å, 9000 Å, 250 Å and Figure 4(b) the variation of the i -layer thickness with a p -layer thickness of 250 Å and an n -layer thickness of 250 Å.

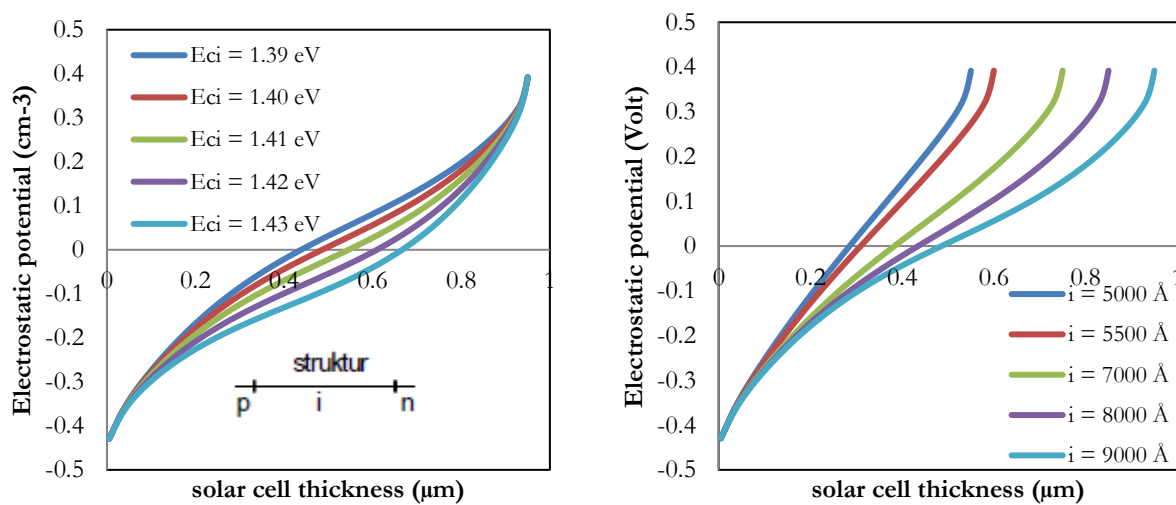


Figure 4. Electrostatic potential profile of μc -Si:H solar cell devices in (a) i -layer optical band gap variation (E_{ci}) and (b) i -layer thickness variation.

Figure 4(a) depicts the variation of the optical band gap value as its electrostatic potential increases from the p -layer to the i -layer and the last to the n -layer. The distribution of electrostatic

potential in the n -layer region is higher when the optical band gap value is at its lowest value of 1.39 eV. It is known that the value of the electrostatic potential is determined more by the concentration of electrons than by the concentration of holes. The greater concentration ratio of the two charge carriers make the higher the electrostatic potential [9]. Since the electric field is an electric potential gradient with respect to position or distance, the electrostatic potential in the i -layer will be higher in the thinner i -layer as a result of the larger electric field between the n -layer and p -layer. The values of electrostatic potential, electron concentration, and hole concentration from the FEMLAB results above are then used in MATLAB to determine the current-voltage (I-V) characteristics of simulated $\mu\text{-Si:H}$ solar cells, by varying the applied voltage.

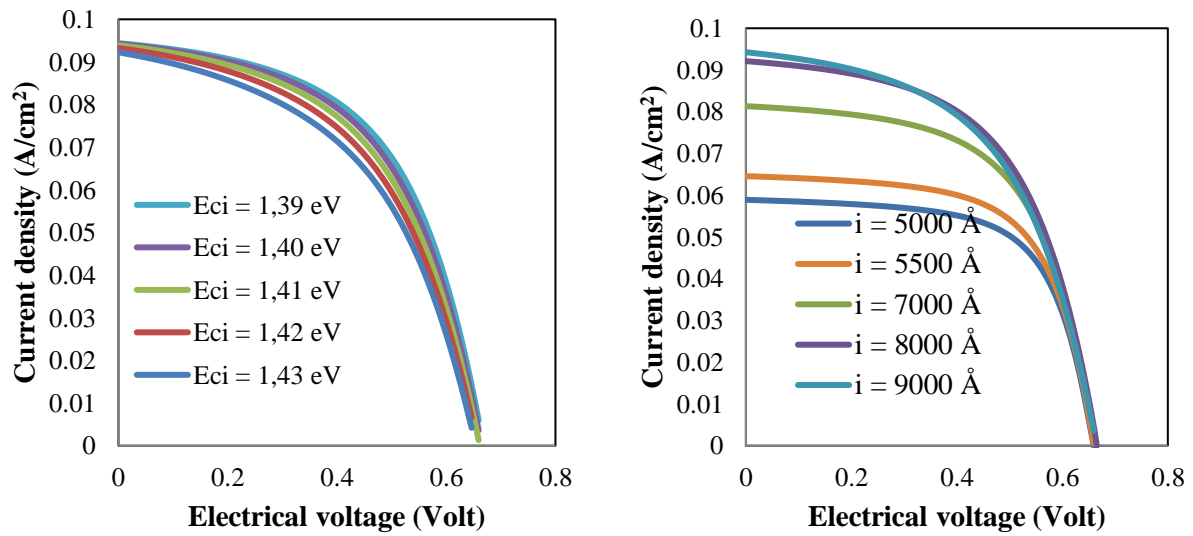


Figure 5. I-V characteristics of $\mu\text{-Si:H}$ solar cells at (a) optical band gap, and (b) variations in i -layer thickness, with a p -layer thickness of 250 Å and an n -layer thickness of 250 Å

Figure 5(a) shows the I-V characteristics of $\mu\text{-Si:H}$ solar cells at variations in the thickness of the i -layer. The solar cells have better characteristics with a smaller i -layer optical band gap, $E_{ci} = 1.39$ eV. These results are in line with the results of research conducted by Nebo [10]. While in Figure 5(b), it appears that the value of the output current density increases with increasing i -layer thickness until it reaches the highest current at i -layer thickness of 9000 Å, the voltage almost does not change.

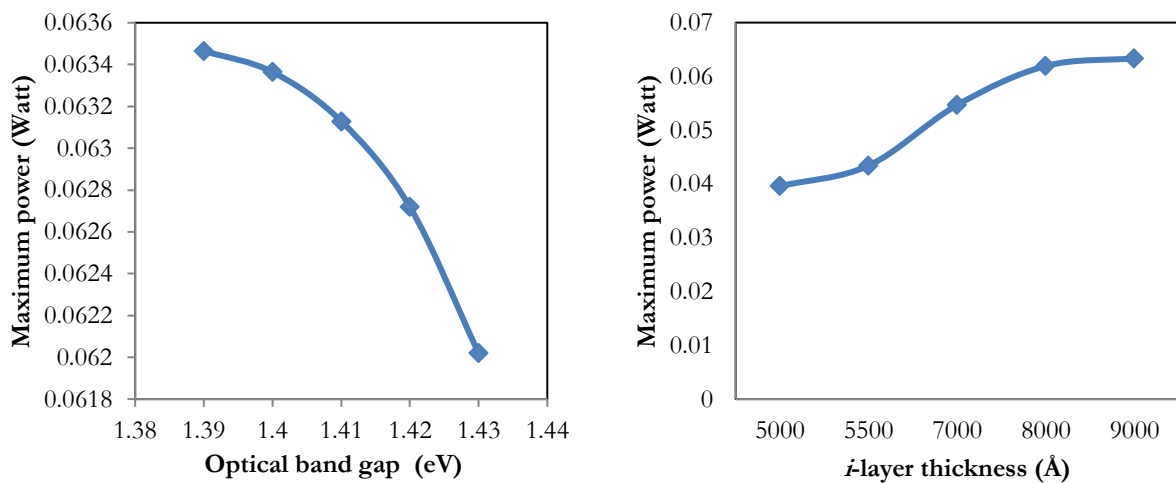


Figure 6. Maximum power of $\mu\text{-Si:H}$ solar cell devices with different i -layer optical bandgap widths, (a) p -layer and n -layer optical band gap width remain at 1.42 eV and 1.5 eV, respectively. (b) with a p -layer thickness of 250 Å and an n -layer thickness of 250 Å

The graph of the solar cell $\mu\text{-Si:H}$ maximum power as a function of the optical band gap is shown in Figure 6(a). From this graph, it can be seen that the maximum power of $\mu\text{-Si:H}$ solar cells varies from 0.06202 Watt to 0.063465 Watt for the variation of the i -layer optical band gap from 1.39 eV to 1.43 eV. From the graph, it can be seen that the maximum power of the $\mu\text{-Si:H}$ solar cell is optimal at the optical band gap of the i -layer solar cell of 1.39 eV, which is 0.063465 Watt. Meanwhile, the graph of the maximum power of solar cells $\mu\text{-Si:H}$ as a function of the thickness of the i -layer is shown in Figure 6(b). From this graph, it can be seen that the maximum power of $\mu\text{-Si:H}$ solar cells varies from 0.039598 Watt to 0.063364 Watt for variations in the thickness of the i -layer from 5000 Å to 9000 Å. The maximum power of the $\mu\text{-Si:H}$ solar cell is optimal at the thickness of the i -layer of the 9000 Å solar cell, which is 0.063364 Watt.

CONCLUSION

Distributed electrons are more effective in $\mu\text{-Si:H}$ solar cells with an i -layer which has a smaller optical band gap, $E_{ci} = 1.39$ eV, so that the rate of recombination of charge carrier pairs occurs faster. This can also be seen from the decrease in hole concentration, where a smaller optical band gap results in a faster decrease in hole concentration. Variations in the thickness of the i -layer appear to only affect the change in the concentration of electrons or holes in the i -layer where the thicker i -layer, which is 9000 Å, has a higher concentration of electrons and holes than the thinner i -layer. The distribution of the electrostatic potential is higher at the thinner i -layer thickness. This is also seen in the higher electrostatic potential distribution in $\mu\text{-Si:H}$ solar cells with an i -layer which has a smaller optical band gap of 1.39 eV. The better characteristics are possessed by solar cells with a smaller i -layer optical band gap of 1.39 eV, while the thickness variation in the i -layer shows an increase in the ability of $\mu\text{-Si:H}$ solar cells along with the addition of the i -layer thickness.

BIBLIOGRAPHY

- [1] Fatema Aabdallah Musa Ahmed, "Structural Properties and Optical Modelling of SiC Thin Films," Department of Physics and Astronomy, University of the Western Cape., Magister Thesis 2020.
- [2] M. Kondo, A. Matsuda M. Isomura, "Device Grade Amorphous Silicon Prepared by High-Pressure Plasma," *Jpn. J. Appl. Phys.*, vol. 41, pp. 1947-1951, 2002.
- [3] Martin A Green, "Third generation photovoltaics: solar cells for 2020 and beyond," *Physica E: Low-dimensional Systems and Nanostructures*, vol. 14, no. 1-2, pp. 65-70, 2002.
- [4] J Meier, E Vallat-Sauvain, N Wyrsh, U Kroll, C Droz, U Graf A V Shah, "Material and solar cell research in microcrystalline silicon," *Solar Energy Materials & Solar Cells*, vol. 78, pp. 469-491, 2003.
- [5] Tomoko Takagi, Setsuo Kaneko Kazushige Takechi, "Performance of a-Si-H Thin Films Transistors Fabricated by Very High Frequency Discharge Silane Plasma Chemical Vapor Deposition," *Jpn. J. Appl. Physics*, vol. 36, no. 1, pp. 6269-6275, 1997.
- [6] A Groß, T Jana, S Ray, A Lambertz, R Carius, F Finger O Vetterl, "Changes in electric and optical properties of intrinsic microcrystalline silicon upon variation of the structural composition," *Journal of Non-Crystalline Solids*, vol. 299-302, pp. 772-777, 2002.
- [7] K Saeful, F Selly D Rusdiana, "Microcrystalline silicon thin film solar cells prepared by hot wire cell method," Universitas Pendidikan Indonesia, Bandung, 2004.
- [8] Youn-Jung Lee, Jinjoo Park, Sunbo Kim, Hyeongsik Park, Sangho Kim Chonghoon Shin, "Current Status of Thin Film Silicon Solar Cells for High Efficiency," *Current Photovoltaic*

Research, vol. 5, no. 4, pp. 113-121, 2017.

- [9] Ida Usman, "Penumbuhan Lapisan Tipis Silikon Amorfi Terhidrogenasi Dengan Teknik HWC-VHF-PECVD dan Aplikasinya Pada Divais Sel Surya," Institut Teknologi Bandung, Disertasi 2006.
- [10] Chimbundu U Nebo, "Understanding $\mu\text{-Si:H}$ solar Cell performance and its optimization using modeling," Delft University of Technology (TU Delft), Delft, Belanda, Master of Science Thesis 2009.
- [11] M Konagai K Takahashi, *Amorphous Silicon Solar Cell*. London: North Oxford Academic Pub. Ltd., 1986.
- [12] Y. Tiandho, W. Sunanda, F. Afriani, A. Indriawati, and T.P. Handayani, "Accurate model for temperature dependence of solar cell performance according to phonon energy ," *Latvian Journal of Physics and Technical Sciences*, vol. 55, no. 5, pp. 15-25, 2018.